Triplet kinase-phosphatase targeting to overcome kinase inhibitor tolerance in brain tumor cells

Oxana V. Denisova[1], Joni Merisaari[1,2], Riikka Huhtaniemi[1], Xi Qiao[1], Laxman Yetukuri[1,3], Mikael Jumppanen[1], Amanpreet Kaur[1], Mirva Pääkkönen[1], Carina von Schantz-Fant[3], Michael Ohlmeyer[5,6], Krister Wennerberg[3,7], Otto Kauko[1], Raphael Koch[8], Tero Aittokallio[3,4,9], Mikko Taipale[10], Jukka Westermarck[1,2]*

Affiliations:

[1]Turku Bioscience Centre, University of Turku and Åbo Akademi University, Turku, Finland.

[2]Institute of Biomedicine, University of Turku, Turku, Finland

[3]Institute for Molecular Medicine Finland (FIMM), HiLIFE, University of Helsinki, Helsinki, Finland.

[4]Centre for Biostatistics and Epidemiology (OCBE), Faculty of Medicine, University of Oslo, Oslo, Norway.

[5]Icahn School of Medicine at the Mount Sinai, NY, USA.

[6]Atux Iskay LLC, Plainsboro, NJ, USA.

[7]Biotech Research & Innovation Centre, University of Copenhagen, Copenhagen, Denmark.

[8]University Medical Center Goettingen, Goettingen, Germany.

[9]Institute for Cancer Research, Department of Cancer Genetics, Oslo University Hospital, Oslo, Norway.

[10]Donnelly Centre, University of Toronto, Toronto, Canada.

*Corresponding author. Email: jukka.westermarck@bioscience.fi

Abstract

Kinase inhibitor tolerance of human glioblastoma is an unmet clinical challenge and a mechanistic enigma. Here, we demonstrate that glioblastoma cell tolerance to multi-kinase inhibition can be reverted by reactivation of Protein Phosphatase 2A (PP2A). To characterize kinase targets of clinical stage multi-kinase inhibitor UCN-01 synergizing with PP2A reactivation, we established a strategy, named Actionable Targets of Multi-kinase Inhibitors (AToMI). AToMI revealed AKT and mitochondrial pyruvate dehydrogenase kinases (PDK1-4) as the co-targets for UCN-01-elicited synthetic lethality with PP2A reactivation. Notably, heterogeneous glioblastoma and medulloblastoma models were tolerant to AKT and PDK1-4 inhibitor monotherapies, and their combinations, but were effectively inhibited by triplet therapy including pharmacological PP2A reactivation. Mechanistically, overcoming the kinase therapy tolerance by the triplet therapy could be explained by combinatorial effects on signaling rewiring between AKT and PDK1-4, decrease in mitochondrial oxidative phosphorylation, and BH3-only protein mediated apoptosis priming. The brain-penetrant triplet combination had a significant *in vivo* efficacy in intracranial glioblastoma and medulloblastoma models. Collectively, we present a generalizable approach to identify actionable co-targets of multi-kinase inhibitors and demonstrate that overcoming of the kinase inhibitor tolerance in brain tumor cells requires triplet targeting of AKT, PDK1-4, and PP2A.

47 # Introduction

48

49 Even though kinase inhibitors have revolutionized cancer therapies, most tumors acquire
50 resistance to kinase inhibitors (1,2). Especially in cancer types genetically associated with
51 hyperactivation of kinase pathways, such as human glioblastoma, the clinically observed
52 kinase inhibitor resistance is a mechanistic enigma (3-5). Acquired therapy resistance
53 develops via two phases - first through adaptive development of a drug-tolerant cellular state,
54 and later, stable resistance that often occurs through acquisition of genetic mutations (6).
55 The emerging evidence strongly indicates that the drug-tolerance is initiated rapidly after
56 drug exposure by non-mutational signaling rewiring, often mediated by phosphorylation
57 dependent signaling pathways (7,8). Thereby, characterization of the phosphorylation-
58 dependent signaling rewiring events, and kinases/phosphatases controlling the rewiring, is
59 expected to provide novel approaches for targeting the tumor relapse at its roots (9).

60

61 In addition to the development of non-genetic therapy tolerance, lack of target specificity of
62 kinase inhibitors is a major translational challenge (2). Recent studies demonstrate that only
63 a few kinase inhibitors target selectively their intended kinase target, and that the therapeutic
64 effects of many kinase inhibitors are mediated by inhibition of other than their assumed
65 target kinase (10,11). The unselectivity of kinase inhibitors can be employed therapeutically
66 in a case the multi-kinase inhibitor (MKI) (12). Of clinically approved MKIs, sunitinib has an
67 FDA approval for the treatment of gastrointestinal stromal tumors and advanced renal cell
68 carcinoma. Additionally, derivatives of the classical MKI staurosporine (STS), have reached the
69 clinics. Midostaurin (PKC412) is approved for the treatment of FLT3-mutated acute myeloid

70 leukemia (12), whereas another STS derivative UCN-01 (7-hydroxystaurosporine), was tested
71 in phase II clinical trials in metastatic melanoma and relapsed T-Cell Lymphomas
72 (NCT00082017). However, it is well established that each of these clinically tested STS
73 derivatives inhibit activities of up to 50 kinases with approximately similar efficiency
74 (10,13,14). Further, the STS derivatives are compromised by their pharmacokinetic properties
75 in a case of brain tumors as they do not cross the brain-blood barrier (BBB). Therefore,
76 development of MKIs towards clinical use would benefit from a better understanding of the
77 kinase targets mediating both the therapeutic and potential toxic effects in each disease
78 application. On the other hand, systematic mapping of the kinase targets of each MKI might
79 provide an opportunity for development of novel combination therapy approaches by
80 combining more selective kinase inhibitors targeting only the preferred kinases with more
81 preferential pharmacokinetic and pharmacodynamic profiles. However, generalizable
82 strategies for analysis of actionable MKI targets are currently missing.
83
84 Glioblastoma (GB) is the most common primary brain tumor in adults associated with high
85 degree of therapy resistance, tumor recurrence and mortality (5,15). Extensive genome-wide
86 profiling studies have established receptor tyrosine kinase RTK/RAS/PI3K/AKT signaling as
87 one of the core altered pathways contributing to GB disease progression (3,16). AKT pathway
88 fuels aerobic glycolysis (17), and GB cells are notorious for employing aerobic glycolysis in
89 energy production and survival (18,19). However, targeting of these deregulated signaling
90 mechanisms have achieved dismal clinical response rates in GB (4,20,21). Furthermore,
91 disappointing results have been obtained from combination of kinase inhibitors, including
92 also the MKIs (21). In addition to challenges with drug delivery across the BBB with a number
93 of kinase inhibitors, the failure of kinase targeted therapies in GB has been proposed to be

94 linked to the prevalence of kinase pathway-mediated rewiring mechanisms (21), and general
95 apoptosis-resistance of glioblastoma stem-like cells (GSCs) (15).
96
97 Protein phosphatase-2A (PP2A) is a ubiquitous serine/threonine phosphatase. Some PP2A
98 complexes act as tumor suppressors and their inhibition is required for human cell
99 transformation (22,23). PP2A regulates several kinase pathways and drug resistance
100 mechanisms, and PP2A inhibition in cancer cells has been shown to drive broad-range kinase
101 inhibitor resistance (24). PP2A is frequently inactivated in GB by non-genetic mechanisms
102 including overexpression of endogenous PP2A inhibitor proteins such as CIP2A, PME-1, SET
103 and ARPP19 (25-27). We recently published proof-of-concept data that reversal of PME-1-
104 mediated PP2A inhibition strongly sensitized GB cells to several kinase inhibitors, including
105 clinically tested STS derivatives (28). However, the translational value of these results
106 remained questionable as PME-1 was experimentally inhibited by siRNAs and STS molecules
107 that do not cross the BBB. Recently, a series of BBB permeable small molecule activators of
108 PP2A (SMAPs) have been developed (29). However, their effects on kinase inhibitor resistance
109 in GB has not yet been addressed.
110
111 To leverage on the therapeutic potential of combination of MKIs with pharmacological PP2A
112 reactivation for GB therapy (28), we established a generalizable multi-step strategy for
113 characterization of Actionable Targets of Multi-kinase Inhibitors (AToMI). The results identify
114 AKT and pyruvate dehydrogenase kinases (PDK1-4) as the targets of MKI UCN-01 in drug-
115 induced synthetic lethality (SL)(30) in combination with PP2A reactivation. As a translationally
116 relevant outcome, we demonstrate that triplet targeting of AKT, PDK and PP2A induced
117 robust synergistic cell death across heterogeneous GB and medulloblastoma (MB) cell lines,

118 and resulted in significant *in vivo* therapeutic effects on intracranial tumor models of GB and
119 MB. Mechanistically, we identify a role for PP2A in regulating mitochondrial metabolism and
120 blunting therapy-induced signaling rewiring. Collectively, these results support the clinical
121 observations that combinations of kinase inhibitors alone are not sufficient for overcoming
122 kinase inhibitor therapy tolerance in brain cancers, but indicate that this can be achieved by
123 further combination of kinase inhibitors with pharmacological reactivation of PP2A.

124 # Results

125

126 **Pharmacological reactivation of PP2A synergizes with a multi-kinase inhibitor UCN-01**

127

128 Based on our previous data demonstrating that PME-1 effects in GB cell kinase inhibitor
129 resistance are mediated by PP2A (28), we hypothesized that the recently developed PP2A
130 reactivating compounds (SMAPs) (29) could provide a pharmacological approach to induce
131 synthetic lethal (SL) drug interaction (30) with UCN-01 in GB cells (Fig. 1A). To test the
132 hypothesis, we directly compared the synergy with UCN-01 and PP2A reactivation by either
133 PME-1 depletion (31), or SMAP (NZ-8-061) treatment, on colony growth potential of T98G
134 cells. As shown in Fig. 1B, PME-1 depletion (either by siRNA or by CRISPR/Cas9) or NZ-8-061
135 did not induce any significant growth defect but induced potent SL with UCN-01. The
136 interaction between NZ-8-061 and UCN-01 was dose dependent and observed by using both
137 compounds at concentrations that showed negligible monotherapy activity (Fig. 1C, D, S1A).
138 Validating the particular potential of PP2A reactivation in kinase inhibitor sensitization (9),
139 NZ-8-061 displayed synergistic activity with as low as 0.5-1 μM concentration, that is
140 approximately 10-fold lower concentrations that has been previously shown to be required
141 for monotherapy effects for the compound (25,32). To rule out that the synergy between NZ-
142 8-061 and UCN-01 would be mediated by any potential non-selective targets of NZ-8-061, we
143 used SMAPs DBK-794 and DBK-1154 derived from dibenzoapine tricyclic family, i.e. chemically
144 different from NZ-8-061 (Fig. 1E). Both DBK-794 and DBK-1154 were originally used to
145 demonstrate direct interaction between SMAPs and PP2A, and for mapping of their
146 interaction region (32). Importantly, these chemically diverse PP2A reactivators all resulted

147 in identical drug interaction with UCN-01 (Fig. 1C, D, F, S1B). Together with identical synergy
148 observed by genetic PP2A reactivation (Fig. 1B) (28), and induction of synergy with non-toxic
149 low micromolar SMAP concentration (Fig. 1D), the use of SMAPs with different chemistry
150 mitigate concerns that the SMAP effects would be related to potential non-selective effects
151 reported using toxic (10-30 μM) concentrations of NZ-8-061 (a.k.a DT-061) (33). Induction of
152 caspase 3/7 activity indicated that the mode of cell death by SMAP+UCN-01 combination was
153 apoptosis (Fig. 1G), and the drug interaction was validated in multiple GB cell lines (Fig. 1H,
154 S1B). Importantly, synergy between UCN-01 and NZ-8-061 was not observed in non-
155 cancerous fibroblasts providing evidence for cancer selectivity of the drug interaction (Fig.
156 S1D). The synergistic drug interaction in GB cells was also seen in hypoxic environment, which
157 is a common resistance mechanism in GB (Fig. S1C).

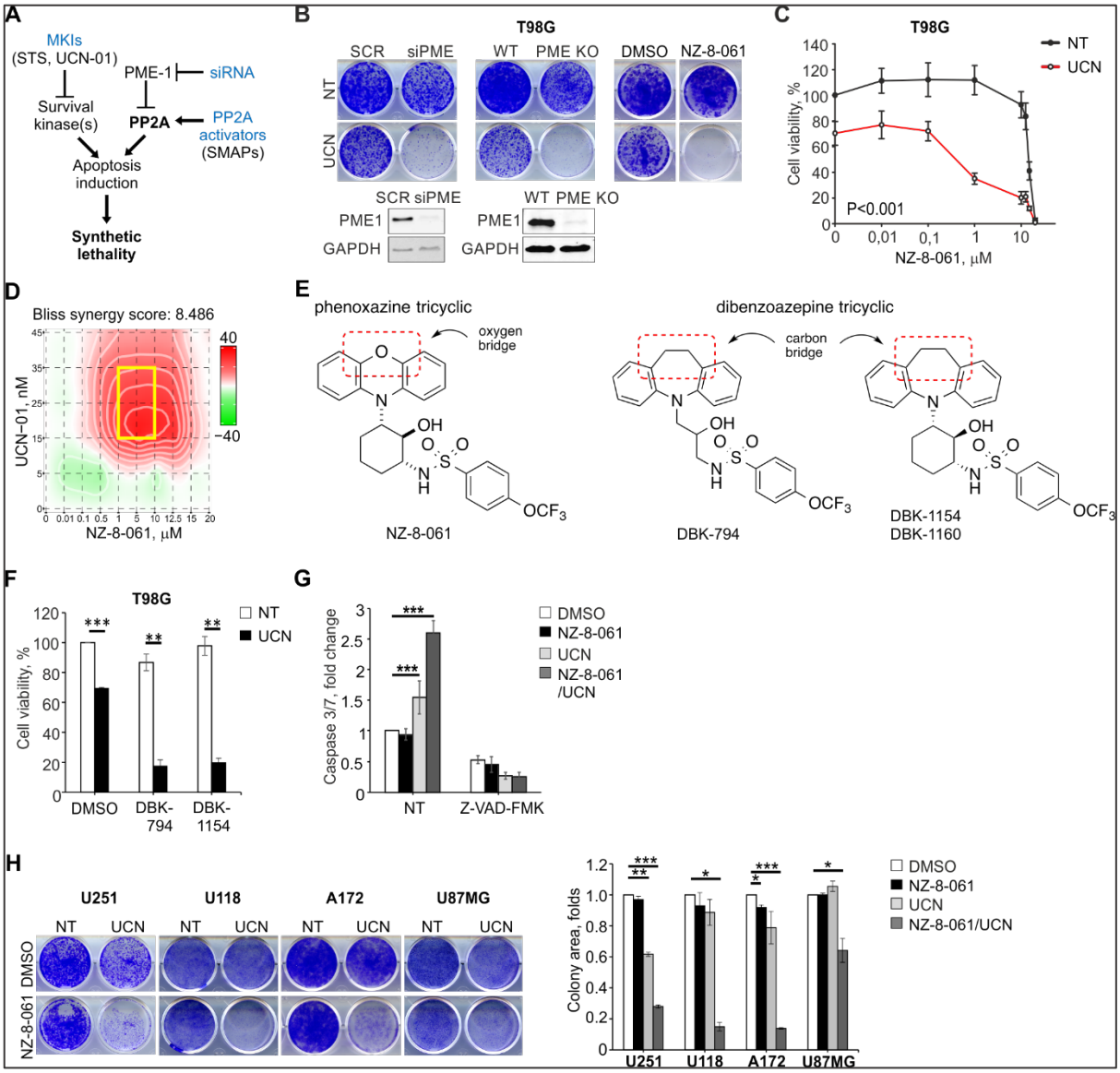

Figure 1. PP2A reactivation and UCN-01 exert a synergistic effect in GB. A) Schematic illustrating PP2A reactivation predisposed to MKI-induced synthetic lethality in GB. **B)** Representative images of colony formation assay in T98G cells under PME-1 siRNA-mediated depletion, PME-1 KO or NZ-8-061 treatment. Cells were treated with 25 nM UCN-01 (UCN) or left untreated (NT). Western blot analysis of PME-1 depletion or KO (lower panel). **C)** Viability of T98G cells treated with increasing concentration of NZ-8-061 either alone or in combination with 25 nM UCN-01 (UCN) for 72 h. Data as mean ± SD (n = 3 independent experiments; ***P < 0.001, Student's *t*-test). **D)** Synergy plot showing the most synergistic area (yellow box) between NZ-8-061 and UCN-01 in T98G cells. The Bliss synergy score is calculated over the whole dose-response matrix. **E)** Structures of two different classes of SMAPs exhibiting similar drug synergy with UCN-01. **F)** Viability of T98G cells treated SMAPs, 10 μM DBK-794 and 5 μM DBK-1154, alone or in combination with 25 nM UCN-01 for 72 h. Data as mean ± SD (n = 2 independent experiments; **P < 0.01, ***P < 0.001, Student's t-test). **G)** Caspase 3/7 activity in T98G cells treated with 8 μM NZ-8-061 alone or in combination

173 with 25 nM UCN-01 (UCN) for 24 h. The caspase inhibitor Z-VAD-FMK (20 µM) was added at
174 the same time. Data as mean ± SD (n = 3 independent experiments; ***P < 0.001, Student's
175 *t*-test). **H)** Representative images (left) and quantified data of colony formation assay (right)
176 in U251, U118, A172 and U87 cells treated with 8 µM NZ-8-061 alone or in combination with
177 UCN-01 (UCN; 200 nM, 25 nM, 50 nM and 500 nM, respectively). Data as mean ± SD (n = 2
178 independent experiments; *P < 0.05, **P < 0.01, ***P < 0.001, Student's *t*-test).
179

180 **Strategy for characterization of Actionable Targets of Multi-kinase Inhibitors (AToMI)**

181

182 Results above demonstrate strong synergistic activity between PP2A reactivation and multi-
183 kinase inhibition by UCN-01. However, as UCN-01 targets approximately 50 different kinases
184 at nanomolar concentrations (10,13), it remains unclear which one(s) of these kinases are
185 involved in SL phenotype observed in combination with PP2A reactivation. To systematically
186 map the UCN-01 co-target interactions, we devised a functional screening platform consisting
187 of the following steps:
188 1) Chaperone interaction assay (34) to compare direct kinase binding between UCN-01 and
189 other STS derivatives displaying differential synergism with PP2A reactivation in GB cells.
190 2) siRNA screening for synergistic interaction between PP2A reactivation and targeting of the
191 individual kinase hits from the step 1.
192 3) Bioinformatics analysis of actionable kinase networks based on steps 1 and 2 for
193 identification of selective small molecule inhibitors for the critical kinase nodes in the
194 network.
195 4) Small molecule kinase inhibitor validation experiments.
196 As this strategy could be generally suitable for functional filtering of targets of MKIs, we
197 hereby refer to the screening platform as characterization of Actionable Targets of Multi-
198 kinase Inhibitors (AToMI) (Fig. 2). The individual technologies used in AToMI are

199 interchangeable with the most suitable technologies for any other application AToMI would
200 be used for.
201
202 **AToMI screening for UCN-01 target kinases involved in GB cell synthetic lethality in**
203 **combination with PP2A reactivation**
204
205 By using AToMI, we compared the kinase target profiles of STS analogues CEP-701, K252a,
206 and UCN-01, previously shown to induce SL in PME-1 depleted T98G cells (28), as well as
207 K252c and Rebeccamycin that did not induce SL when combined with PP2A reactivation (28).
208 The differential synergistic activities of these STS derivatives in combination with NZ-8-061
209 was confirmed by colony growth assay (Fig. S2A). All five compounds were screened for their
210 direct kinase protein binding against 300 kinases by chaperone interaction assay (34) (Fig. 2A,
211 S2B, Table S1). This assay measures the interaction of kinases with their chaperone Cdc37 in
212 the presence (or absence) of kinase inhibitors. Binding of the inhibitor to its target leads to
213 thermodynamic stabilization of the target, which can be detected as weaker interaction
214 between the kinase and Cdc37 (35).Using log2 -0.5-fold reduction in chaperone binding as a
215 threshold for interaction, a total of 29 candidate kinases were identified to differentially
216 interact with STS derivatives that synergized with PP2A (CEP-701, K252a, and UCN-01), but
217 not with rebeccamycin or K252c (Table S2).
218
219 In the siRNA screening step of AToMI, the goal was to identify among the shared targets of
220 CEP-701, K252a, and UCN-01, individual kinases whose co-inhibition resulted in a synergistic
221 inhibition of cell viability with PP2A reactivation (Fig. 2B). The screen was conducted with a
222 custom human kinase siRNA library, which had three non-overlapping siRNAs targeting each

223 kinases. In addition to 29 candidate kinases from the step 1, the siRNA library was extended
224 to include 8 additional kinases frequently altered in GB (3,16) (Table S3). The siRNAs were
225 reverse transfected to T98G cells, and cells were subsequently exposed to PP2A reactivation
226 by NZ-8-061 treatment (Fig. 2B). In the validation screen, we included selected 25 kinases in
227 combination with PME-1 siRNA to evaluate similarity in drug sensitization between chemical
228 (NZ-8-061) and genetic (PME-1 siRNA) PP2A reactivation (Fig. 2B). The efficacy of PME-1
229 depletion by tree independent siRNAs was validated by western blotting from parallel
230 samples (Fig. S2C). For each kinase siRNA, Gene Activity Ranking Profiles and synergy scores
231 were computed as described in the methods section of siRNA screens. Notably, regardless of
232 the marked differences in the targeting approaches, most of the kinases targeted in both
233 screens were found to synergize both with NZ-8-061 treatment and PME-1 depletion (Fig.
234 2D), validating both the shared PP2A-induced mode of action, and the broad impact of PP2A
235 activity in kinase inhibitor tolerance in GB.
236
237 STRING protein-protein interaction network analysis of the AToMI SL kinases from the step 2
238 revealed enrichment of RTK/RAF/MAPK (PDGFR, RAF1, BRAF, MAPK1) and PI3K/AKT/mTOR
239 pathways (PIKCA, AKT1, AKT3), as well as mitochondrial pyruvate dehydrogenase kinase
240 (PDK1 and PDK4) among the kinases, connected to PP2A B-subunits, previously shown to
241 mediate SL between STS and PME-1 depletion (Fig. 2E) (28). As each of these kinase modules
242 were represented also among the kinases that were shared between the NZ-8-061 and siPME-
243 1 synergy targets, we proceeded to testing these GB signaling nodes by selective small-
244 molecule inhibitors. Selectivity of the chosen small-molecule inhibitors was evaluated based
245 recently published target selectivity databases, and for some compounds also by Chaperone
246 interaction assay (Table S4) (10,14). To facilitate translation of the results, we also considered

247 oral bioavailability and BBB permeability of the compounds in drug selection. The selected 7
248 kinase inhibitors were screened for cell viability effects in T98G cells with two SMAPs, NZ-8-
249 061 and DBK-1154 (25). As a control, we used an inactive SMAP analog DBK-766, that binds
250 PP2A but is unable to reactivate it even at a concentration of 20 μM *in vitro* (32). The results
251 show that both NZ-8-061 and DBK-1154 sensitized T98G cells to MK-2206 and AKT1/2i (AKT
252 signaling) (36), and DCA (PDK1-4 inhibitor) (19,37) used at concentrations that engage their
253 aimed target kinase (Fig. S2D, E). Importantly, the inactive SMAP (DBK-766) did not synergize
254 with any of these kinase inhibitors (Fig. 2F). Further, RAF inhibitors (LY3009120 and
255 Vemurafenib), PI3K inhibitor (LY294002), or MINK1 inhibitor (mubritinib) did not display
256 significant combinatorial effect with PP2A reactivation (Fig. 2F). Importantly, another PDK
257 inhibitor, lipoic acid (37), recapitulated the synergy with SMAPs (Fig. S3A, B). In addition,
258 further validating the role of PP2A as a target for SMAPs in inducing the synergistic drug
259 interaction, PP2A reactivation by PME-1 inhibition also synergized with MK-2206 and DCA
260 treatments (Fig. S3C, D).
261
262 Collectively, these results demonstrate the usefulness of AToMI screening for identification
263 of individual actionable target kinases for MKIs. Regarding the UCN-01 target kinases involved
264 in SL with PP2A reactivation, AToMI screening resulted in selection of pharmacological
265 inhibitors of AKT pathway and mitochondrial PDK1-4 kinases for further functional validation.
266

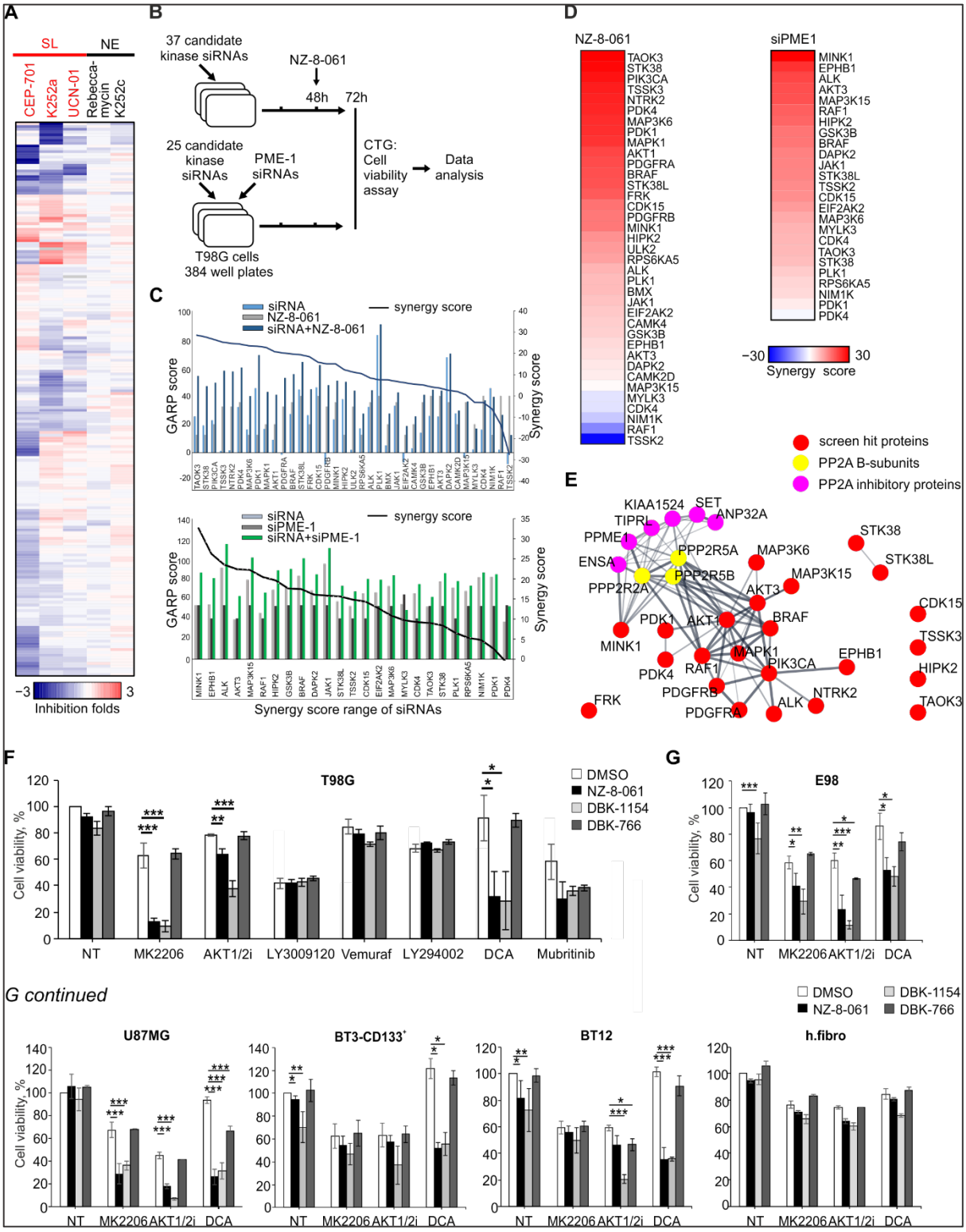

Figure 2. AToMI screening for UCN-01 target kinases involved in GB cell synthetic lethality in combination with PP2A reactivation. A) Heat map representation of interaction of STS derivatives, CEP-701, K252a, UCN-01, rebeccamycin and K252c, with 300 protein kinases by chaperone interaction assay. Color scale bar indicates log2 fold changes of kinase/Cdc37 interactions between inhibitor and DMSO treatments. SL - synthetic lethality, NE - no effect. **B)** Schematic illustrating of the performed kinase siRNA screens in T98G cells under NZ-8-061-

274 treatment or PME-1 depletion. **C)** GARP scores of siRNA screen in T98G cells under NZ-8-061-
275 treatment or PME-1 depletion (left axis). Kinases were ordered according to synergy scores
276 (right axis). **D)** Heat map representation of kinases involved in synthetic lethality in NZ-8-061-
277 treated and PME-1-depleted T98G cells. Color bar indicates the synergy scores. **E)** STRING
278 interactive mapping of screen kinase hits onto PP2A network. **F)** Viability of T98G cells and **G)**
279 established GB, E98 and U87MG, and patient-derived GSCs, BT3-CD133^{+} and BT12, cell lines
280 treated with the selected kinase inhibitors alone or in combination with 8 µM NZ-8-061, 6 µM
281 DBK-1154 or 10 µM DBK-766 for 72 h. Human fibroblasts were used as a negative control cell
282 line. Data as mean ± SD (n = 3 independent experiments). *P < 0.05, **P<0.01, ***P<0.001
283 by Student's *t*-test.
284

285 **Triplet therapy induces cytotoxicity across heterogeneous GB cell lines**

286

287 Cellular heterogeneity and high intrinsic therapy resistance of glioblastoma stem-like cells
288 (GSCs) are major challenges related GB therapies (15). Therefore, we evaluated the synergy
289 between AKT and PDK inhibitors with SMAPs across two additional established GB cell lines,
290 and two patient-derived mesenchymal type GSC lines (BT-CD133^{+}, BT12) (25,38). Notably,
291 western blot analysis revealed constitutive, but highly heterogeneous AKT and PDK1-4 activity
292 across most of the brain tumor cell models used in this study (Fig. S4A). Consistently with high
293 intrinsic kinase inhibitor resistance of GB cells (25,39), none of the kinase inhibitors as
294 monotherapies, and used at doses that effectively inhibited their intended targets (Fig. S2D,
295 E), did induce cytotoxic response (Fig. 2G). Further, albeit combination with SMAPs sensitized
296 GB and GSC cells to a certain extent to AKT or PDK1-4 inhibition, the maximal co-inhibition of
297 cell viability with double combinations was highly variable across the cell lines, and only some
298 instances could be considered cytotoxic (Fig. 2G). Notably, the inactive SMAP analog DBK-766
299 did not synergize with any tested kinase inhibitor in any of the GB cell lines, and the human
300 fibroblasts did not show any signs of synergy between kinase inhibition and SMAPs (Fig. 2G).
301

302 As these results indicate that single kinase inhibitors, even when combined with PP2A
303 reactivation, cannot be used as a general strategy against heterogeneous GB cell populations,
304 we decided to combine both AKT pathway and PDK1-4 inhibition together with PP2A
305 reactivation as a triplet therapy. The rationale behind the triplet combination was that non-
306 genetic signaling rewiring induced by single therapies (7,8) could be avoided by simultaneous
307 targeting of two major kinase signaling nodes and by lowering the serine/threonine
308 phosphorylation activity by PP2A. Even though both AKT inhibitors exhibited similar
309 efficiency, we chose MK-2206 for the triplet therapy because of its frequent use in clinical
310 trials (36). To assess long-term cytotoxic effects of the combinations, the triplet therapies
311 were tested by using colony growth assays. Notably, fully supportive of therapy-induced
312 therapy tolerance, all cell lines, except for T98G, were found to be resistant to cytotoxic
313 effects of combined PDK (DCA) and AKT (MK-2206) inhibition (Fig. 3A, B). NZ-8-061 was found
314 to potentiate effects of MK-2206 or DCA variably across the cell lines; most notably seen in
315 E98 cells for MK-2206, and in BT3-CD133^{+} cells for DCA (Fig. 3A, B). However, the triplet
316 therapy was the only drug combination that was found effectively eradicating all GB and GSC
317 lines without notable effects on fibroblasts (Fig. 3A, B). This supports our hypothesis that
318 triplet therapy is needed to tackle the heterogeneity of the therapy responses in GB.

319

320 Medulloblastoma (MB) is another brain tumor in which kinase inhibitors have been proven
321 clinically ineffective (40). However, AKT, PDK and PP2A have all been implicated as potential
322 targets for future MB therapies (40,41). Therefore, we studied whether the results above
323 could be expanded from GB to MB. Reassuringly, when tested on two MB cell models, DAOY
324 and D283-Med, representing SHH subtype and Group 3/4, respectively, we observed similar

325 synergistic drug interaction between MK-2206, DCA and SMAPs (NZ-8-061 and DBK-1160) as
326 across the GB cell lines (Fig. 3C). In addition, in colony growth assay in DAOY cells, we
327 confirmed that combination of AKT and PDK inhibition was not sufficient for potent
328 cytotoxicity, whereas combination with SMAP DBK-1160 resulted in very potent SL phenotype
329 (Fig. 3D).

330

331 To better understand the qualitative differences between GB cell responses to mono, double,
332 and triplet therapies, we performed an Incucyte long-term confluency analysis in E98 cells
333 treated with drugs twice for two weeks, with one week drug holiday in between (Fig. 3E).
334 Although the E98 cells responded to all therapies during the first dosing period, the long-term
335 data confirmed full resistance to each of the monotherapies. On the other hand, doublet
336 combinations were found to be more efficient than monotherapies, but with all doublet
337 combinations the effect was only cytostatic, as the cells were able to regain their proliferation
338 after the drug wash-outs (Fig. 3E, see days 6-13 and 21-24). However, the triplet therapy
339 treated cells were not able to escape the therapy during the follow-up and showed clear signs
340 of cytotoxic response after initiation of the second dosing period (Fig. 3E, F).

341

342 Collectively, these results provide a strong validation to the AToMI screening results across
343 genetically heterogeneous GB, GSC and MB cell lines. Importantly, the results clearly
344 demonstrate that efficient shutdown of therapy tolerance across GB and MB cell lines
345 requires combined inhibition of two kinases, and reactivation of PP2A phosphatase activity.

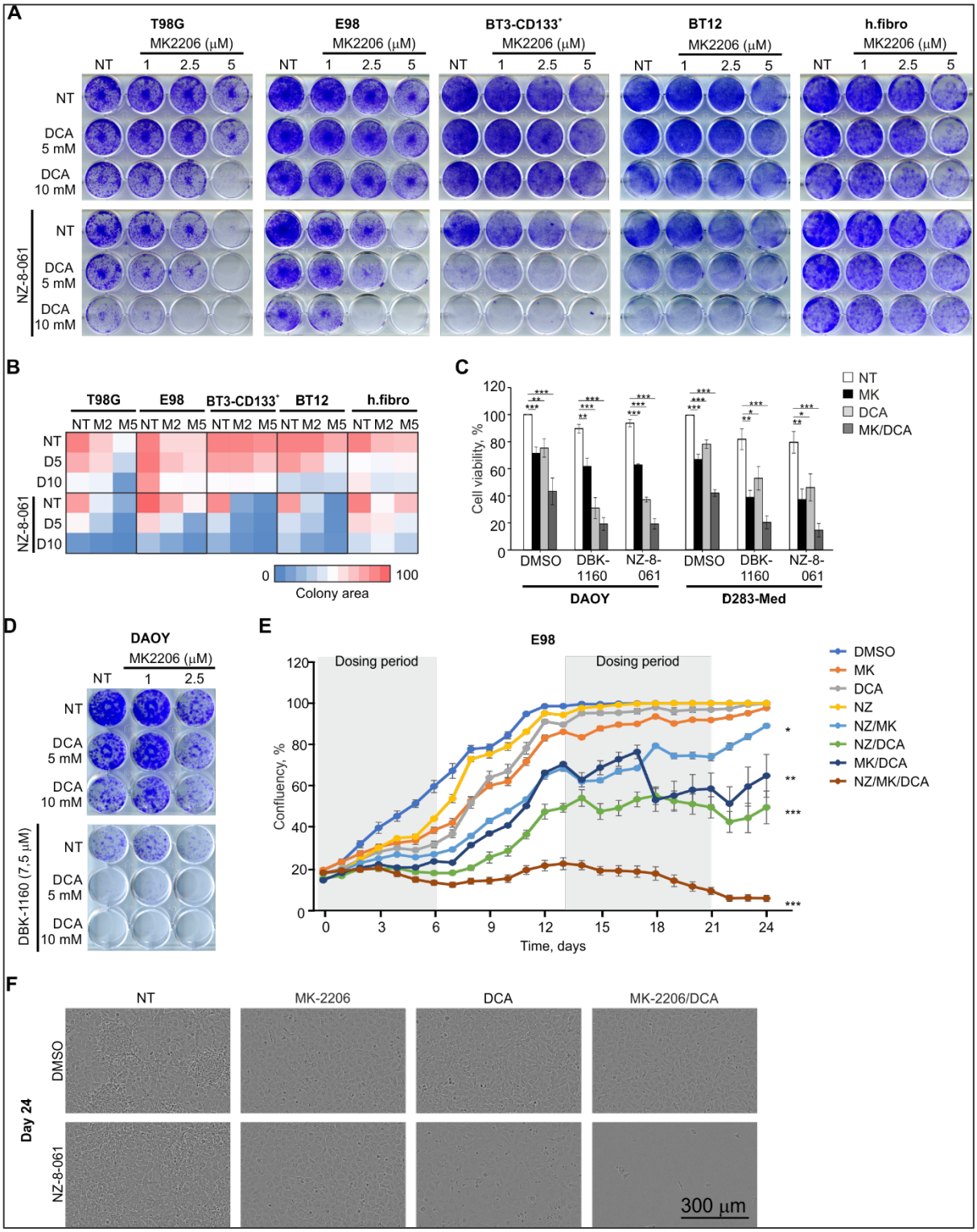

346

347 **Figure 3. Triplet combination of NZ-8-061 with DCA and MK-2206 exert a synergistic**
348 **cytotoxic effect in molecularly heterogeneous GB and MB cell lines. A)** Representative
349 images of colony growth assay in T98G, E98, BT3-CD133^{+}, BT12 and fibroblasts under triplet
350 combination treatment as indicated. **B)** Heat map representation of quantified colony growth
351 assay data in the indicated cell lines treated with MK-2206 (MK; 2.5 or 5 µM), DCA (D; 5 or 10
352 mM) or NZ-8-061 alone or in double or triplet combination. Human fibroblasts were used as

353 a negative control cell line (n=2 independent experiments). **C)** Cell viability in DAOY and D283-
354 Med medulloblastoma cells treated with DMSO, 8 µM DBK-116 or 10 µM NZ-8-061 alone or
355 in combination with 5 µM MK-2206 (MK), 20 mM DCA, or MK + DCA for 72 h. Data as mean ±
356 SD (n = 3 independent experiments: *P<0.05, **P<0.01, ***P<0.001 by Student's t-test). **D)**
357 Representative images of colony growth assay in DAOY cells under triplet combination as
358 indicated. **E)** Proliferation of E98 cells treated with DMSO, 7 µM MK-2206 (MK), 20 mM DCA,
359 10 µM NZ-8-061 (NZ) alone or in double or triplet combinations. Data as mean ± SEM (n = 6 –
360 12 wells per condition). *P < 0.05, **P<0.01, ***P<0.001 by Kruskal-Wallis test to DMSO
361 group. **F)** Representative pictures of E98 cells from (E) at day 24.
362

363 **The triplet therapy blunts therapy-induced signaling rewiring and potentiates apoptosis**
364 **induction**

365

366 Fully consistent with the therapy-induced signaling rewiring hypothesis, we found that while
367 MK-2206 efficiently inhibited the AKT S473 phosphorylation, it simultaneously enhanced, at
368 least to certain extent in all cell lines, phosphorylation of a direct mitochondrial PDK1-4 target
369 PDHE1α (Pyruvate Dehydrogenase E1 Subunit Alpha 1) (37) (Fig. 4A-C). In contrast, inhibition
370 of PDK by DCA completely abolished phosphorylation of PDHE1α S300, but enhanced
371 phosphorylation of AKT in T98G cells (Fig. 4A-C). However, combination of MK-2206 and DCA
372 was able to shut-down phosphorylation of both proteins across all cell lines (Fig. 4A-C). NZ-8-
373 061 treatment instead affected AKT and PDK signaling in very heterogeneous manner,
374 depending on the kinase inhibitor combination, and the cell line. In other cell lines, except for
375 T98G, DCA + NZ-8-061 combination inhibited AKT S473 phosphorylation, but instead resulted
376 in less efficient PDHE1α S300 inhibition than with DCA alone (Fig. 4C). On the other hand, NZ-
377 8-061 did rescue the compensatory PDHE1α S300 phosphorylation induced by MK-2206. NZ-
378 8-061 also expectedly inhibited AKT phosphorylation across the cell lines, but very
379 interestingly also synergized with DCA in AKT inhibition (Fig. 4A-C).

380

381 To correlate these findings to the apoptotic potential of the combination therapies, we
382 examined PARP cleavage from the same cellular lysates. The data reveals that neither NZ-8-
383 061 at doses that synergize in drug combinations, nor total shutdown of AKT and PDK
384 signaling (MK-2206 + DCA) (Fig. 4B, C), was alone sufficient for maximal apoptosis induction
385 in any of the studied GB cell lines (Fig. 4D). However, the highest apoptotic response was
386 consistently seen across all cell lines upon the triplet therapy treatment (Fig. 4D). Lastly, DAOY
387 MB cells displayed similar therapy-induced signaling rewiring between AKT and PDK pathways
388 than in GB cells, but combination with DBK-1160 blunted the rewiring and resulted in potent
389 apoptosis induction (Fig. S4B).
390
391 Collectively, these observations confirm prevalent therapy-induced signaling rewiring and
392 heterogeneity in the combinatorial drug responses across the GB cells. Importantly, SMAP
393 treatment was found to inhibit therapy-induced signaling rewiring, and thereby convert
394 cytostatic kinase inhibitor responses to cytotoxic effects across GB cells. The results also
395 strongly indicate that the discovered kinase pathway inhibition tolerance mechanism is
396 shared between GB and MB.

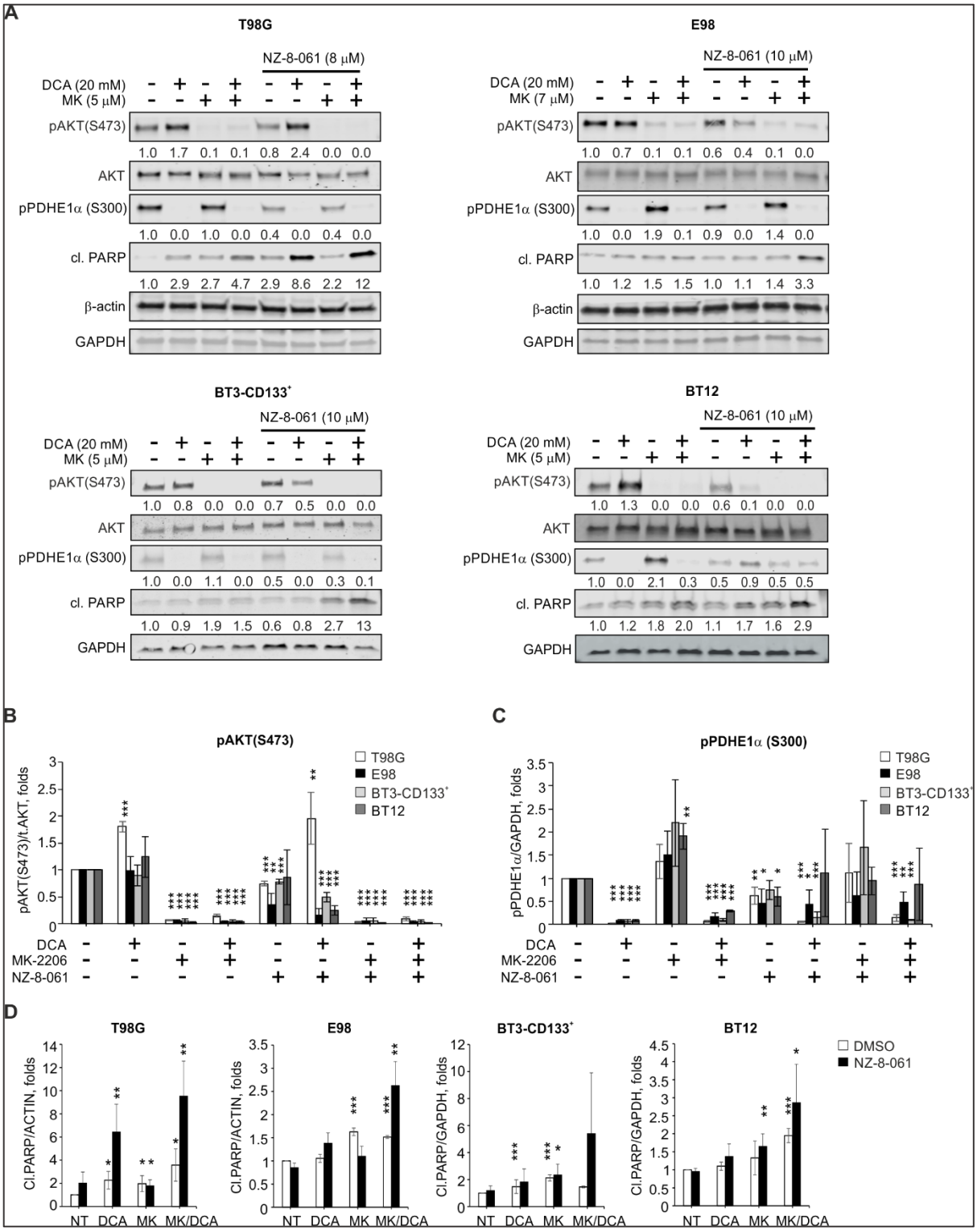

Figure 4. Inhibition of drug-induced signaling rewiring and apoptosis sensitization by the triplet therapy. A) Immunoblot assessment of phosphorylated AKT (S473), phosphorylated PDHE1α (S300), and cleaved PARP after treatment with MK-2206 (MK), DCA or NZ-8-061 alone or in double or triplet combination for 24 h in T98G, E98, BT3-CD133^{+} and BT12 cells. Normalized quantifications from (A) for **B)** phosphorylated AKT (S473) to total AKT, **C)**

403 phosphorylated PDHE1α to GAPDH, and **D)** cleaved PARP to β-actin. Data as mean ± SD (n = 3
404 independent experiments: *P < 0.05, **P<0.01, ***P<0.001 by Student's *t*-test).
405

406 **Triplet therapy inhibits mitochondrial OXPHOS and primes to BH3 protein-mediated**
407 **apoptosis**

408

409 The above results revealed an interesting crosstalk between cytoplasmic AKT and
410 mitochondrial PDK1-4 signaling. PP2A inhibition by CIP2A was recently implicated in
411 regulation of mitochondrial oxidative phosphorylation (OXPHOS) (42). Specifically, PP2A
412 reactivation by CIP2A inhibition resulted in inhibition of maximal mitochondrial respiration,
413 decrease in spare oxidative capacity, and decrease in ATP production (42). To analyze whether
414 apoptosis-sensitizing effect of pharmacological PP2A reactivation observed above would be
415 associated with defects in OXPHOS, the T98G cells were exposed to either MK-2206 or DCA
416 alone, or in combination with NZ-8-061, and analyzed by Seahorse Real-Time XF Analyzer (see
417 Materials and Methods for details). As excepted, DCA alone increased ATP production, as it
418 reactivates the OXPHOS in the mitochondria (Fig. 5A, B) (37,43). On the contrary, MK-2206
419 reduced ATP production and mitochondrial-linked respiration (Fig. 5B). Interestingly, NZ-8-
420 061 used at SL inducing non-toxic concentration had a broad-spectrum effect on
421 mitochondrial metabolism. Especially interesting drug interaction was inhibition of DCA-
422 induced OXPHOS (Basal, Maximal, and Spare), indicating that PP2A reactivation can prevent
423 compensatory mitochondrial survival mechanism. NZ-8-061 alone, and in combination with
424 MK-2206, also profoundly increased proton leak indicating for mitochondrial membrane
425 damage (Fig. 5A, B).

426

427 Based on recently published results, the inner mitochondrial impairment on OXPHOS, and
428 increased proton leakage, potently interact with BH3-only protein mediated apoptosis
429 regulation in the outer mitochondrial membrane (44). Therefore, we also characterized the
430 impact of drug combinations on mitochondrial cytochrome *c* release. In line with other
431 findings (Fig. 3C and 4D), we observed limited cytochrome *c* release by single drug treatment
432 with NZ-8-061, DCA or MK-2206 or with double NZ-8-061 + DCA or NZ-8-061 + MK-2206
433 combinations (Fig. 5C). In contrast, the triplet therapy induced strong cytochrome *c* release
434 (Fig. 5C). As cytochrome *c* release is controlled by BH3-only proteins on the outer
435 mitochondrial membrane (45), we eventually wanted to clarify the functional interaction
436 between cytoplasmic AKT, and mitochondrial PDK1-4 kinases on regulation of mitochondrial
437 apoptosis by dynamic BH3 profiling. BH3 profiling uses a library of synthetic peptides to
438 elucidate mechanisms by which cell evade apoptosis and dissect the functional relevance of
439 each BCL2 family member (46,47). BH3 profiling revealed a limited impact on apoptotic
440 priming by PDK1-4 inhibition, but a marked increase in the cells' susceptibility towards BIM,
441 HRK, and MS1 mediated cytochrome *c* release when AKT was inhibited (Fig. 5D). Notably,
442 there was a marked enhancement and broadening of BH3-mediated apoptosis priming when
443 AKT and PDK1-4 were co-inhibited, providing an additional explanation for their synergistic
444 pro-apoptotic effect (Fig. 5E). Results related to the impact of triplet therapy on BH3 profiling
445 were inconclusive presumably due to high apoptotic activity (data not shown).
446
447 Collectively, these data identify multiple mitochondrial converge points between AKT, PDK1-
448 4 and PP2A signaling. They also reveal the mechanistic basis for the high apoptotic activity of
449 the triplet therapy due to NZ-8-061-elicited inhibition of the compensatory OXPHOS, and
450 inner mitochondrial membrane proton leakage, combined with synergism between MK-2206

451 and DCA on BH3 priming. Notably, the synergistic interaction between inner mitochondrial

452 dysfunction (OXPHOS and proton leakage) and BH3 priming in apoptosis induction is

453 consistent with recent findings in other cancer types (44).

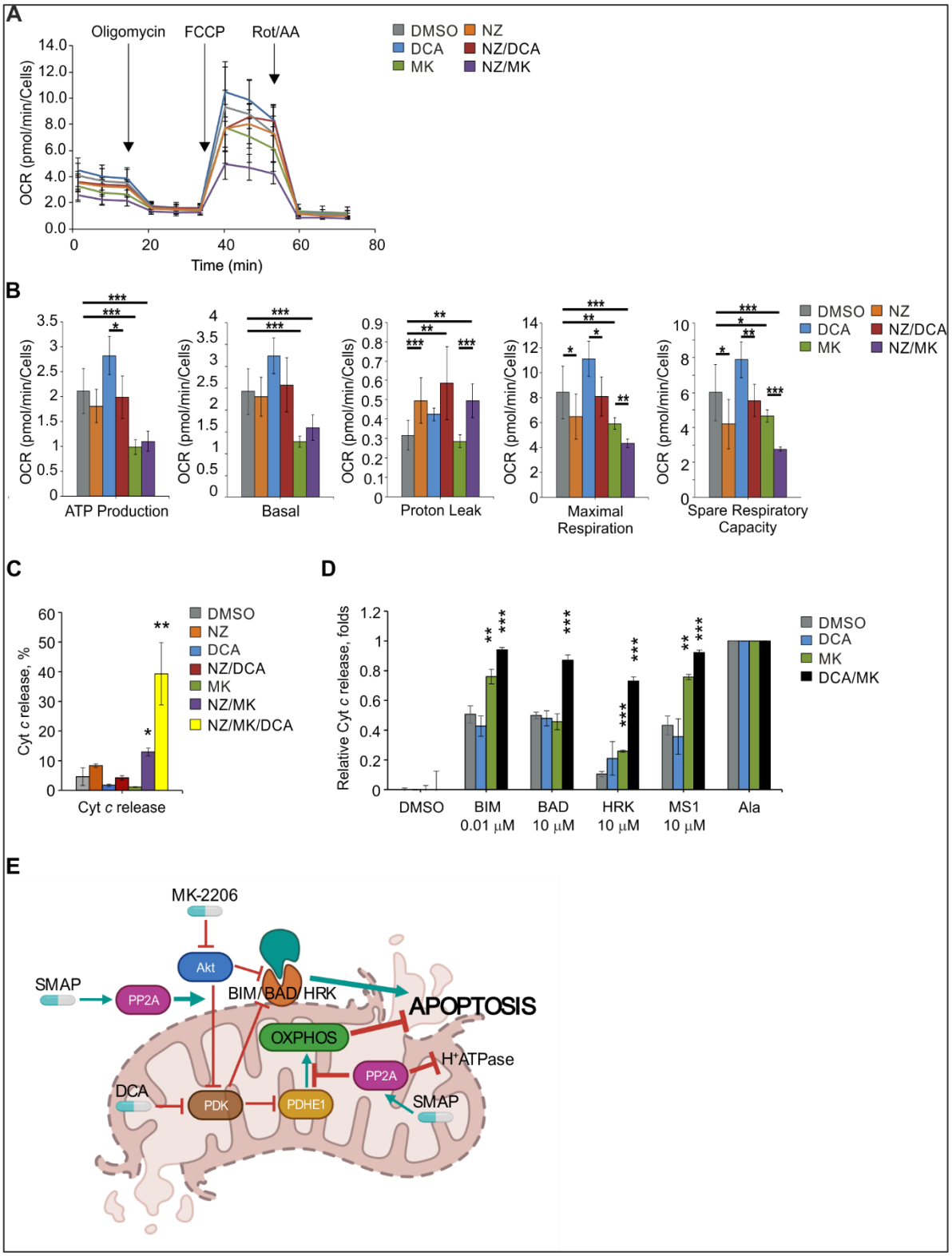

454

455 **Fig. 5. Triplet therapy inhibits mitochondrial OXPHOS and primes to BH3 protein-mediated**
456 **apoptosis A)** Mitochondrial stress test Seahorse profile in T98G cells treated with 10 mM DCA
457 or 7 µM MK-2206 (MK) alone or in combination with 10 µM NZ-8-061 (NZ) for 24 h. **B)**
458 Mitochondrial parameters from (A). Data as mean ± SD (n = 3 independent experiments; *P <
459 0.05, **P<0.01, ***P<0.001 by Student's t-test). **C)** Cytochrome c release from T98G cells
460 treated with 5 µM MK-2206 (MK), 20 mM DCA or 8 µM NZ-8-061 (NZ) alone or in double or
461 triplet combination for 24 h. Data as mean ± SD (n = 3, *P < 0.05, **P<0.01, ***P<0.001 by
462 Student's *t*-test). **D)** Priming of T98G cells to apoptosis induction by indicated BH3 peptides.
463 5 µM MK-2206 (MK), 20 mM DCA were used alone or combination for 24 h. Data as mean ±
464 SD (n = 3, *P < 0.05, **P<0.01, ***P<0.001 by Student's *t*-test) **E)** Schematic illustration of
465 mitochondrial mechanisms for triplet therapy-induced apoptosis based on Fig. 4 and 5.
466 Inhibition of PDK1-4 induces compensatory OXPHOS but this is blunted by SMAP treatment
467 which additionally induces mitochondrial membrane proton leakage. PDK1-4 and AKT
468 inhibition synergizes on BH3-meidated apoptosis priming and SMAP treatment inhibits
469 signaling rewiring between the kinases. Whereas in response to doublet drug combinations
470 cells can induce some compensatory survival mechanism, these are simultaneously inhibited
471 in triplet therapy treated cells resulting in terminal apoptosis induction.
472

473 **Validation of therapeutic potential of the triplet therapy in orthotopic GB and**
474 **medulloblastoma models**

475

476 *In vivo* relevance of the results was investigated in subcutaneous and intracranial models
477 using both E98 GB cells and DAOY MB cells. First, we wanted to provide *in vivo* validation to
478 AToMI screening results that the SL effects of SMAPs with UCN-01 can be recapitulated by
479 combination of AKT and PDK inhibition. As UCN-01 does not cross the BBB, these experiments
480 were performed using subcutaneous xenografts, and instead of NZ-8-061, we used DBK-1160
481 as a SMAP due to its better pharmacokinetic profile based on our previous studies (data not
482 shown). Fully validating the results from AToMI approach, the orally dosed triplet therapy
483 (DBK-1160 + MK-2206 + DCA) was equally efficient, or even superior to combination of DBK-
484 1160 and UCN-01 (Fig. 6A, B). The robust *in vivo* antitumor effect of the triplet therapy in
485 DAOY model was readily seen also when comparing the sizes of the excised tumors (Fig. 6C).

486

487 To molecularly profile the triplet therapy effect in the treated tumors, the vehicle and the
488 triplet therapy treated tumors (n=5 for both) were subjected to mass spectrometry
489 phosphoproteomics analysis using TMT-labeling. Upon filtering the data for those
490 phosphopeptides there were quantifiable from at least three tumors per group, and with FDR
491 of 5% for significance of the difference in phosphopeptide expression between the groups
492 (Table S5), the Reactome pathway analysis validated the impact triplet therapy on both
493 apoptosis and cell cycle, but on the other hand revealed a very strong enrichment of targets
494 involved in "Signaling by Rho GTPases" (Fig. 6D, S5, Table S6). Furthermore, fully consistent
495 with our model that efficient therapy response in brain tumors requires wide-spread kinase
496 inhibition, we found inhibition of phosphorylation of several kinases from the triplet therapy
497 treated tumors (Fig. 6E, Table S5). Notably, among those were inhibition of the
498 phosphorylation of the activation loop of AKT1, 2 and 3, which together with enrichment of
499 mTOR signaling based on phosphopeptide data (Fig. 6E, Table S5), perfectly supports our
500 mechanistic data demonstrating importance of the shutdown of rewiring to AKT signaling (Fig.
501 4). Inhibition of AKT signaling was evident also based on kinase target motif enrichment
502 analysis where canonical AKT target motifs (R-x-R-x-x-S/T and R-x-x-S/T) were clearly enriched
503 in the phosphopeptides downregulated by the triplet therapy (Fig. 6I). Beside AKT, among the
504 dephosphorylated kinases were also the pro-survival downstream targets of ERK MAPK, RSK1
505 and 3, as well as transcriptional elongation promoting kinase CDK9, that is essential for brain
506 tumor-initiating cells (48), and a synergistic drug target with SMAPs (49). Additional
507 exploration of the data by NetworKIN analysis, revealed enrichment of CDK1 and CDK5 targets
508 (Fig. S6A). CDK5 is a known neuronal kinase activated in GB and MB, and CDK1 regulation links
509 very well to enrichment of cell cycle/mitosis based on phoshopeptide data (Fig. 6D).

510 Interestingly, but consistent with the therapy-induced non-genetic signaling rewiring, we also
511 identified a number phosphopeptides upregulated in the triplet therapy treated tumors (Fig.
512 6F; upper right corner and Table S5). Related to kinase signaling, we noticed that several
513 kinases involved in the pro-apoptotic JNK and p38 MAPK signaling were hyperphosphorylated
514 in the treated tumors (Fig. S6B), and both JNK1 and JNK2 were among the top enriched kinase
515 target motifs based on NetworKIN analysis (Fig. S6A). As both JNK and p38 are involved
516 apoptosis regulation by BH3 proteins (50), these data provide a plausible link between the
517 proposed mechanism for triplet therapy induced brain tumor cell killing (Fig. 5E), and the
518 observed in vivo therapeutic effects (Fig.6F).
519
520 Finally, in intracranial model the triplet therapy was tested on luciferase-expressing E98 cells
521 that carry characteristics of GSCs and has very infiltrative growth pattern *in vivo* (25). In
522 addition to these faithful human GB characteristics, E98 cells displayed indistinguishable
523 triplet therapy response as compared to patient derived GSC cell lines *in vitro* (Fig. 3).
524 Importantly, we observed significant inhibition of tumor growth by orally dosed triplet
525 therapy initiated upon appearance of detectable tumors at day 10 (Fig. 6G). For DAOY cells,
526 we relied on mouse survival as the end-point measurement of the therapy effect, since no
527 tumor growth visualization approaches were available for these tumors. Remarkably, more
528 than 50% of the vehicle treated mice died during the therapy, whereas in the triplet therapy
529 group only one mouse had to be sacrificed due to neurological symptoms (Fig. 6H). Following
530 cessation of therapy after 30 days, due to local regulations, we observed a significant increase
531 in mouse survival in the triplet therapy group, associated with 26-day prolongation of the
532 median probability of survival (Fig 6H). No obvious toxicities were observed during triplet
533 therapy treatment periods in either subcutaneous or intracranial models (Fig. S7). However,

534 as expected, the SMAP treatment resulted in reversible increase in liver weight, as has been

535 reported earlier (32).

536

537 Collectively, the subcutaneous tumor results provide *in vivo* validation that AKT and PDK are

538 the target kinases for the SL-inducing effect of UCN-01 in PP2A reactivated brain tumor cells.

539 The results further validate the translational relevance of the results in independent

540 orthotopic tumor models of common human brain tumors.

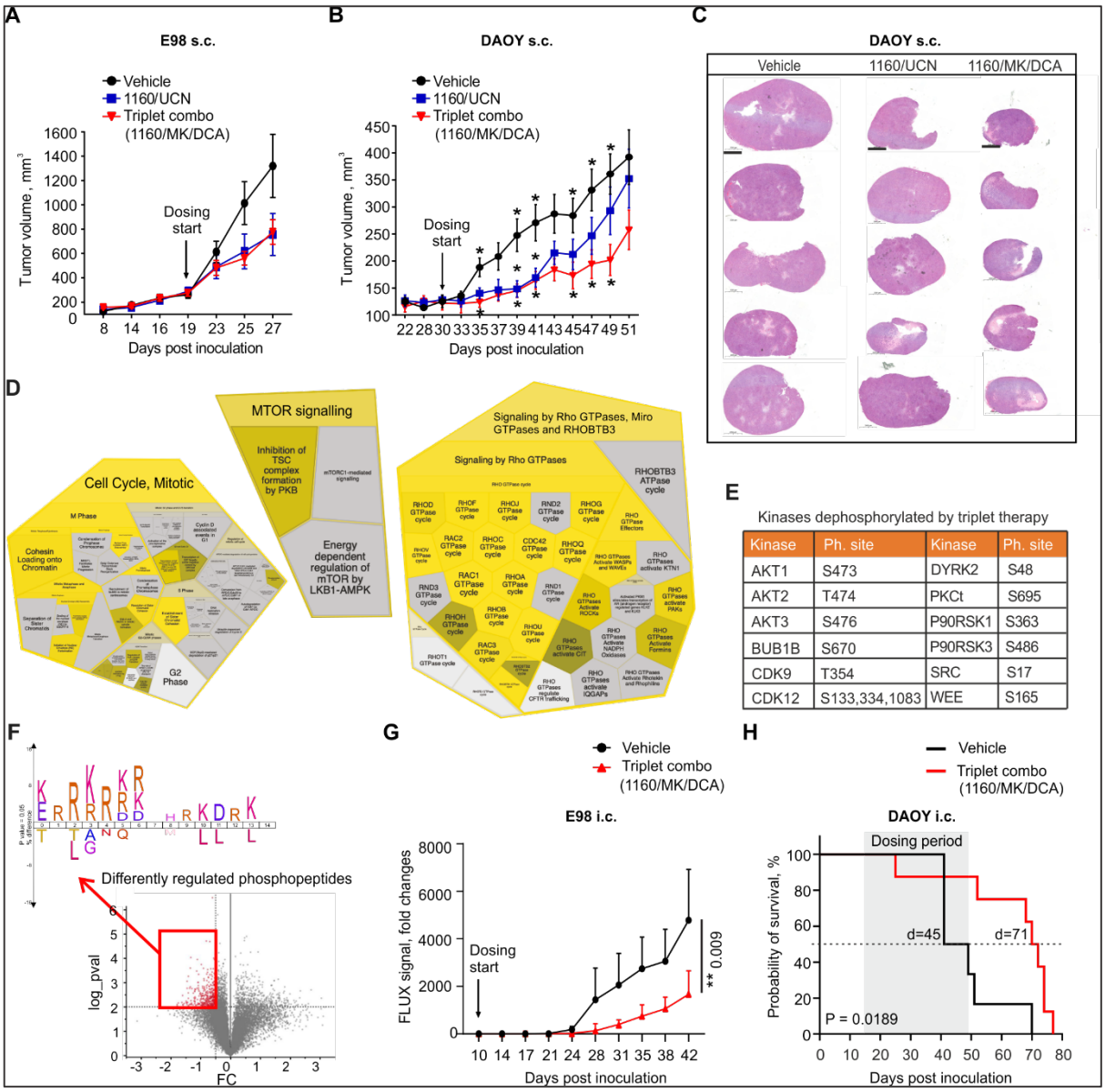

541

542 **Fig. 6. Validation triplet combination therapy in vivo. A-B)** Quantification of tumor volume
543 from E98 (A) and DAOY (B) s.c. tumors in mice treated with DBK-1160 (1160; 100 mg/kg twice
544 a day) and UCN-01 (UCN; 3 mg/kg once a day) or MK-2206 (MK; 100 mg/kg every second day)
545 and DCA (100 mg/kg twice a day), or vehicle control. Each group had n=8 mice in E98, n=10
546 mice in DAOY experiments. Mean ± SD. *P < 0.05 by two-way ANOVA test. **C)** Representative
547 images from H&E staining of DAOY s.c. tumors from (B, n=5). Scale bar, 1000 µm. **D)** Reactome
548 processes based on significantly (p< 0.05) regulated phosphopeptides from triplet therapy
549 treated DAOY xenografts in (B). **E)** Kinases dephosphorylated by triplet therapy in DAOY
550 xenografts from (B). **F)** Volcano plot showing differentially regulated phosphopeptides from
551 (B). Icelogo kinase motif enrichment analysis from the dephosphorylated peptides (in red)
552 (p≤0.01, log2FC ≤ -0.5) revealed enrichment of canonical AKT sites (R-x-R-x-x-S/T and R-x-x-
553 S/T). **G)** Bioluminescence follow up of an orthotopic E98 glioblastoma tumor comparing the
554 vehicle or triplet combination therapies (DBK-1160 (100 mg/kg twice a day) + MK-2206 (100
555 mg/kg every second day) + DCA (100 mg/kg twice a day)). Mean ± SEM. (n=10 mice per group).
556 **P < 0.01 by Student's t-test. **H)** Kaplan–Meier survival analysis of xenograft orthotopic DAOY
557 model treated with triplet combination (DBK-1160 (100 mg/kg twice a day) + MK-2206 (100
558 mg/kg every second day) + DCA (100 mg/kg twice a day)). Vehicle n=6, Triplet combo n=8
559 mice per group. Mantel-Cox test. * P <0.05.

560 ## Discussion

561

562 Kinase inhibitor resistance of brain tumors is a notable unmet clinical challenge (4,21,40).
563 Considering that hyper activated kinase signaling is one of the hallmarks of GB (3,15), clinical
564 resistance of GB to kinase inhibitors constitutes a mechanistic enigma. One of the potential
565 reasons for ineffectiveness of kinase inhibitors in inhibition of oncogenic phosphorylation in
566 GB is that phosphatases have not been taken into the account when designing the GB therapy
567 strategies. There is a very strong theoretical basis for synergistic activities of simultaneous
568 kinase inhibition and phosphatase activation in phosphorylation-dependent cancers (9,29),
569 but the therapeutic impact of such combinatorial approach in overcoming therapy tolerance
570 in brain cancers has been thus far unclear. Our results, using a panel of heterogeneous GB
571 and MB cell lines, provide convincing proof-of-principle evidence that overcoming kinase
572 inhibitor tolerance in brain cancers requires simultaneous multi-kinase inhibition and PP2A
573 phosphatase activation.

574

575 MKIs provide an attractive approach to simultaneously inhibit several oncogenic kinases, and
576 some MKIs (e.g., Sunitinib, PKC412), are clinically used as cancer therapies (12). However,
577 similar to more selective kinase inhibitors, all tested MKIs have thus far failed in GB clinical
578 trials (4). STS derivatives targeting more than 50 kinases (13) could provide a wide enough
579 polypharmacological kinase inhibitor spectrum to target GB driver mechanisms, even in the
580 case of heterogeneous GB cell populations. However, use of STSs as GB therapeutics is
581 compromised by their inability to cross BBB. To overcome these limitations, and to better
582 understand GB relevant STS target kinases, we developed the AToMI approach. As a result,

583 we found 29 kinases which selectively bound to STS derivatives and synergized with PP2A
584 reactivation by either PME-1 inhibition or by SMAPs (Fig. 2A, S2B). Notably, the kinases which
585 synergized with PP2A reactivation represent the commonly hyper activated pathways in GB.
586 For example, AKT pathway is one of the most dysregulated pathways in GB, and it was well
587 presented in the siRNA screen as depletion of AKT1, AKT3 and PIK3CA all synergized with PP2A
588 reactivation (Fig 2C, D). Another strongly GB associated signaling mechanism was
589 mitochondrial glycolysis, as depletion of both PDK1 and PDK4 synergized with PP2A
590 reactivation (Fig 2C, D). PDK kinases are key regulators of metabolic shift from OXPHOS to
591 glycolysis, which promotes GB tumor growth and resistance to therapies (18,19). However,
592 similar to other kinase inhibitor therapies, also AKT and PDK1-4 targeting monotherapies have
593 failed to demonstrate significant survival effects in clinical trials for GB (37,51-53). Our
594 subsequent kinase inhibitor combination experiments, using inhibitors at doses that inhibit
595 their target kinases, validate the ineffectiveness of AKT and PDK1-4 targeting in eradicating
596 heterogeneous GB cell lines (Fig. 3A, B). While all double therapies tested here, involving
597 either two kinase inhibitors, or one kinase inhibitor combined with SMAP, resulted at best in
598 cytostatic effect, the triplet therapy induced cytotoxic response considered as clinically
599 efficacious (Fig. 3A, B). Collectively, these results validate the usefulness of AToMI approach
600 for future studies aiming to characterize actionable targets of MKIs in different indications.
601 The AToMI approach also facilitated the identification of BBB permeable kinase inhibitors
602 with similar biological activity than UCN-01. This allowed validation of all main conclusions of
603 this study *in vivo* in two brain cancer orthotopic models displaying both significant therapeutic
604 effect with the triplet therapy.
605

606 Phosphorylation-dependent signaling rewiring after therapy is a prevalent mechanism for
607 cancer cells to escape apoptotic cell killing (7,8). Consistent with this model, we found that
608 AKT inhibition by MK-2206 induced phosphorylation of the PDK1-4 target PDHE1α in GB and
609 MB cells (Fig. 4A-B, S4B). We also validate *in vivo* inhibition of signaling rewiring to AKT and
610 mTOR in triplet therapy treated MB tumors (Fig. 6D-F). Notably, the therapy-induced signaling
611 rewiring between AKT and PDK pathways was abolished when MK-2206 and DCA were
612 combined, yet it failed to induce efficient apoptosis across the GB and MB cell lines, except
613 for the most sensitive T98G cells (Fig. 3A-C, 4D). PP2A reactivation by SMAPs altered brain
614 tumor cells response to MK-2206 and DCA in multiple ways. Consistent with the established
615 role of PP2A as an AKT phosphatase (23), SMAPs reduced the basal AKT S473 phosphorylation,
616 but surprisingly also strongly synergized with DCA in AKT dephosphorylation in most of the
617 studied cell lines. In addition, PP2A reactivation inhibited signaling rewiring by restraining MK-
618 2206-induced PDHE1α S300 phosphorylation. Interaction between PP2A and PDK was also
619 observed at the level of mitochondrial metabolism. NZ-8-061 decreased basal, spare, and
620 maximal respiratory capacity, and blunted the DCA-induced increase in OXPHOS. Importantly,
621 previous data indicate OXPHOS induction in response to inhibition of glycolysis (such as is
622 seen in DCA-treated cells) as a rescue mechanism protecting cells from apoptosis (54).
623 Furthermore, NZ-8-061 caused mitochondrial inner membrane proton leak which decreases
624 mitochondrial membrane potential leading to higher probability of apoptosis (55).
625
626 Collectively, our data identity a strategy for killing of heterogeneous brain tumor cells based
627 on MKI combined with PP2A reactivation. Specifically, through AToMI approach we identify
628 AKT and PDK1-4 as the critical UCN-01 target kinases involved in synthetic lethality when
629 combined with either genetic or pharmacological PP2A reactivation. Notably, our results are

630 relevant across heterogeneous GB and MB models including patient-derived GSCs. Further,
631 PP2A activation was found to sensitize GB cells against majority of the kinases tested by the
632 AToMI approach (Fig. 2D), hence providing a rich source for kinase inhibitor combinations to
633 be validated in the future studies. Combined with the previously demonstrated role for PP2A
634 in impacting lung cancer cell responses to over dozens of kinase inhibitors (24), our results
635 indicate that the uniform kinase inhibitor resistance observed in GB and MB clinical trials (4),
636 could be to significant extent contributed to non-genetic PP2A inhibition by its inhibitor
637 proteins (25,28,40,56). In this regard, diagnostic definition of PP2A inhibitor protein status
638 would greatly simplify biomarker-based analysis of PP2A activity in brain tumors because it
639 sidesteps the need for analyzing all the possibly relevant PP2A subunits. Specifically, the
640 current results encourage future brain tumor clinical trials with combinations of clinically
641 tested AKT and PDK1-4 inhibitors (20,51,53) in a significant proportion of brain cancer
642 patients with low tumor expression of PME-1 (28). Finally, our results strongly indicate that
643 rapidly developing PP2A reactivation therapies (29) will constitute an attractive future
644 therapy option for brain tumors when combined with multi-kinase inhibition.
645

646 # Methods

647

648 **Cell culture and reagents**

649 Established human GB cell lines U87MG (gift from Ari Hinkkanen, University of Eastern
650 Finland, Joensuu, Finland), A172, U118, U251 (gift from Pirjo Laakkonen, University of
651 Helsinki, Helsinki, Finland), E98-FM-Cherry (gift from William Leenders, Radboud Institute for
652 Molecular Life Sciences, Nijmegen, The Netherlands) and human fibroblasts (gift from
653 Johanna Ivaska, Turku Bioscience, Turku, Finland) were cultured in DMEM (Sigma-Aldrich).
654 T98G (VTT Technical Research Centre, Turku, Finland), DAOY (ATCC) and D283-Med (ATCC)
655 were cultured in Eagle MEM (Sigma-Aldrich). All growth mediums were supplemented with
656 10% (except fibroblasts supplemented with 20%) of heat-inactivated fetal bovine serum (FBS)
657 (Biowest), 2 mM L-glutamine and penicillin (50 U/mL)/ streptomycin (50 µg/mL). All cell
658 cultures were maintained in a humified atmosphere of 5% CO_2 at 37°C.

659

660 The patient-derived GSCs BT3-CD133$^+$and BT12 (Kuopio University Hospital, Kuopio, Finland)
661 (25,38) were cultured in DMEM/F12 (Gibco) and supplemented with 2 mM L-glutamine, 2%
662 B27-supplement (Gibco), penicillin (50 U/mL) / streptomycin (50 µg/mL), 0.01 µg/mL hFGF-β
663 (Peprotech), 0.02 µg/mL hEGF (Peprotech) and 15 mM HEPES-buffer (Gibco). For assays
664 requiring adherent cell, such as colony growth, GSC populations were cultured on Matrigel
665 (Becton Dickinson) coated plates.

666

667 The following chemicals were purchased from indicated distributors: AKT1/2 inhibitor,
668 staurosporine, CEP-701, UCN-01, PKC412, sodium salt of dichloroacetate (DCA) and lipoic acid

669 from Sigma-Aldrich; FRAX486 and Vemurafenib from SelleckChem; K252a and rebeccamycin
670 from Enzo Life Sciences; K252c from Tocris Bioscience; MK-2206 from MedChemExpress.
671 Compound were dissolved in DMSO (Sigma-Aldrich) or mQ (for DCA) and stored at -20°C.
672 SMAPs (NZ-8-061, DBK-794, DBK-1154, DBK-1160 and DBK-766) were kindly supplied by Prof.
673 Michael Ohlmeyer (Icahn School of Medicine at the Mount Sinai, NY, USA), were dissolved in
674 DMSO and stored at room temperature protected from light.

675

676 **Cell viability assay**

677 Optimized numbers of cells (2.5 x 10^3 to 5 x 10^3) were plated onto 96-well plates (Perkin
678 Elmer) and allowed to adhere. After 24 hours, cells were treated with vehicle (DMSO) or the
679 indicated concentrations of compounds. After 72 hours, cell viability was measured using
680 CellTiter-Glo assay (Promega) according the manufacturer's instructions using a BioTek
681 Synergy H1 plate reader (BioTek).

682

683 **Colony formation assay**

684 Optimized numbers of cells (3 x 10^3 to 10 x 10^3) were seeded in either 12-well plates and
685 allowed to adhere. Matrigel matrix coated plates were used for patient-derived glioma stem
686 cells. After approximately 24 hours cells were treated with drugs. After 72 hours of
687 incubation, drug-containing media were replaced with non-drug containing medium and
688 incubated until the control wells were confluent. Cells were fixed with ice cold methanol and
689 stained with 0.2% crystal violet solution in 10% ethanol for 15 min at room temperature.
690 Plates were dried and scanned with Epson Perfection V700 Photo scanner. Quantification of

691 colonies were done with ImageJ by using the Colony area plugin (57). Data were normalized
692 and presented as a per cent of the control.
693
694 Colony formation assays at hypoxic conditions were performed in InvivO2 400 incubator
695 (Ruskinn Technology) at following conditions 1% O_2, 5% CO_2 and 90% humidity.
696
697 **Caspase-3 and -7 activity assay**
698 T98G cells (2.5 x 10^3) were plated in 96-well plates (Perkin Elmer) and allowed to adhere. After
699 24 hours, cells were treated with drugs for the next 24 hours. Pan-caspase inhibitor Z-VAD-
700 FMK (10 mM, Promega) was added at the same time as drugs. Caspase-3 and -7 activity was
701 measured by Caspase-Glo 3/7 Assay (Promega) according the manufacturer's instructions
702 using a BioTek Synergy H1 plate reader.
703
704 **Western blotting and antibodies**
705 Standard immunoblotting analysis was performed using the following primary antibodies:
706 AKT (Cell Signaling, 9272S, 1:1,000), phospho Akt S473 (Cell Signaling, 9271, 1:1,000), PME-1
707 (Santa Cruz, sc-20086, 1:1,000), β-actin (Sigma-Aldrich, A1978, 1:10,000), phospho PDHE1-A
708 type I (S300) (Millipore, ABS194, 1:1,000), cleaved PARP1 (E51) (Abcam, ab32064, 1:1,000)
709 and GAPDH (Hytest, 5G4cc, 1:10,000). Secondary antibodies were purchased from LI-COR,
710 mouse (926-32212) and rabbit (926-68021). The membranes were scanned using an Odyssey
711 scanner (Li-Cor Biosciences). Quantification of protein abundance was assessed with Image
712 Studio Lite (version 5.2) on three immunoblots from independent lysates.
713
714 **Chaperone binding assay**

715 LUMIER (LUminescence-based Mammalian IntERactome) with BACON (bait control) assay
716 was performed as previously described (35). In short, 3xFLAG-tagged bait proteins are
717 transfected into 293T cells expressing the Chaperone-Renilla (prey) luciferase in a 96-well
718 plate. After two days, cells are treated with kinase inhibitors (or DMSO) for 1 hour before cell
719 lysis. The cell lysates expressing each bait protein are applied to anti-FLAG coated 384-well
720 plates, which captures the bait protein. The amount of luminescence in the well, after
721 washing off nonspecifically binding proteins, indicates the interaction between the bait
722 protein with the prey protein. After the luminescence measurement, the amount of bait
723 protein is measured with ELISA, using a different, polyclonal anti-FLAG antibody conjugated
724 to horseradish peroxidase.
725
726 **Long-term growth assay**
727 E98 cells (3 x 10^3) were plated into 96-well plate. On the next day cells were treated with
728 DMSO, MK-2206 (7 µM), DCA (20 mM), NZ-8-061 (10 µM) alone, or in their double or triplet
729 combinations (6-12 wells/condition). Every 3-4 days medium was replaced with fresh media
730 with or without drugs. The confluency of the wells was determined daily using IncuCyte ZOOM
731 live cell analysis system (Essen Bioscience).
732
733 **Mitochondrial respiration measurement**
734 Agilent Seahorse XF Cell Mito Stress Test (Agilent Seahorse Bioscience) was applied to T98G
735 cells according the manufacturer's instructions. In short, T98G cells were seeded at 1 x 10^4
736 cells per well in a Seahorse 96-well XF Cell Culture microplate in 100 µL of the growing
737 medium. On the next day cells were treated with DMSO, DCA (10 mM), MK-2206 (7 µM) alone
738 or in combination with NZ-8-061 (10 µM) for the next 24 hours. On the day of analysis, the

739 growth media were replaced with 120 µL of XF assay media (non-buffered DMEM
740 supplemented with 10 mM glucose, 1 mM sodium pyruvate and 2 mM glutamine) and
741 incubated at 37°C in a non-CO_2 incubator for one hour before running assay. Mitochondrial
742 function of the cells was analyzed by sequential injections of modulators, oligomycin,
743 carbonyl cyanide-4 (trifluoromethoxy) phenylhydrazone (FCCP), and rotenone/antimycin A,
744 at Seahorse XFe96 analyzer (Agilent Seahorse Bioscience). The Seahorse XF Mito Stress Test
745 Report Generator was used to calculate the Seahorse XF Cell Mito Stress Test parameters
746 from Wave software (version 2.6.153). The data were normalized to total protein per well
747 using BCA assay (Thermo Fisher Scientific).
748
749 **BH3 profiling**
750 BH3 profiling was performed as previously described (46,47). In brief, T98G cells were
751 pretreated with DMSO, MK-2206 (5 µM), DCA (20 mM), NZ-8-061 (8 µM) alone, or in their
752 double or triplet combinations for 24 hours. On the next day, cells were permeabilized with
753 0.002% digitonin and treated with a library of synthetic peptides. Peptides used were BIM at
754 0.01 µM, BAD, HRK and MS1 at 10 µM. The BIM peptide assesses the functionality of BAX and
755 BAK. BAD binds and antagonizes BCL-2, BCL-xL, BCL-W, and BFL-1. HRK specifically binds and
756 antagonizes BCL-xL. MS1 binds and antagonizes MCL-1. A pore-forming peptide, alamethicin
757 (positive control), or DMSO (negative control) served as controls. Cells were incubated with
758 the peptides for half an hour at 25°C and subsequently fixed with 4% paraformaldehyde for
759 10 min. Finally, intracellular cytochrome *c* was stained with an immunofluorescence-labeled
760 antibody (BioLegend Alexa Fluor 647 anti-Cytochrome *c* Antibody, clone 6H2.B4). Relative
761 cytochrome *c* release was assessed by formula 1 – [(sample-pos.ctrl.)/(neg.ctrl.-pos.ctrl.)].
762

763 **Bioinformatics analysis**

764 Cytoscape network analysis software (version 3.9.0) (58) was used to visualize the STRING
765 interactive map of hit kinases (59). For calculation and visualization of synergy scores, dose-
766 response matrix of NZ-8-061 and UCN-01 combination data were applied to SynergyFinder
767 (version 2.0) web-application (60).

768

769 **Statistical analyses**

770 For cell culture experiments, three biological replicates have been performed, and each
771 condition was tested in triplicate, unless otherwise specified. Data are presented as mean ±
772 SD and statistical analyses were carried out using a two-tailed Student's t-test assuming
773 unequal variances. For *in vivo* experiments, the following statistical tests were chosen
774 depending on the results of the preliminary Shapiro-Wilk test of data normality. Two way
775 ANOVA with Tukey's multiple comparisons test were used to assess differences between
776 three or more experimental groups. Lonk-rank (Mantel-Cox) test was used in survival analysis.
777 These univariate statistical analyses were performed using GraphPad Prism 9 software
778 (GraphPad Software). $P < 0.05$ was considered statistically significant.

779

780 **Supplementary Materials**

781 Supplementary Methods and Figures S1-7.

782 Table S1. Chaperone interaction assay data.

783 Table S2. 28 kinase hit list.

784 Table S3. The customer kinase siRNA library.

785 Table S4. Inhibitor selectivity data.

786 Table S5. Significantly ($p < 0.05$) regulated phosphopeptides from triplet therapy treated
787 DAOY xenografts.
788 Table S6. Enriched Reactome pathways based on Table S5.
789 Table S7. The list of the used siRNA.
790
791 **Competing interests**
792 Authors declare no competing interests.
793
794 **Authors' Contributions**
795 Conception and design: O.V.D., J.M., A.K. J.W. Development of methodology: O.V.D., J.M.,
796 R.H., X.Q., J.W. Experimental work: M.T., O.V.D., C.S-F., K.W. R.K., M.P., O.K. Bioinformatic
797 analysis: M.J., L.Y., O.K., T.A. In vivo work: O.V.D., J.M., R.H. Resources: M.O. Writing: O.V.D.,
798 J.M., T.A., J.W.
799
800 **Acknowledgements**
801 Authors want to acknowledge Turku Center for Disease Modelling (TCDM) and Made
802 Consulting for expert help with mouse experiments, Artur Padzic for help and expertise with
803 lentivirus experiments, William Eccleshall and Mung Kwan Long for help with Seahorse
804 experiments, and Kari Kurppa for expert help with Incucyte experiments and for helpful
805 discussions. Johanna Ivaska is thanked for comments on the manuscript. Taina Kalevo-Mattila
806 is acknowledged for excellent technical support as well as the entire Turku Bioscience
807 personnel for excellent working environment.
808
809

Funding

Project was funded by Jane and Aatos Erkko Foundation, Finnish Cultural Foundation, Sigrid Juselius Foundation, K.Albin Johanssons Foundation, AAMU Suomen Lasten Syöpäsäätiö, Turku Doctoral Programme of Molecular Medicine, Academy of Finland, and Finnish Cancer Foundation.

815 # References

816 1. Cohen P, Cross D, Janne PA. Kinase drug discovery 20 years after imatinib: progress
817 and future directions. Nat Rev Drug Discov **2021**;20(7):551-69 doi 10.1038/s41573-
818 021-00195-4.
819 2. Attwood MM, Fabbro D, Sokolov AV, Knapp S, Schioth HB. Trends in kinase drug
820 discovery: targets, indications and inhibitor design. Nat Rev Drug Discov
821 **2021**;20(11):839-61 doi 10.1038/s41573-021-00252-y.
822 3. Brennan CW, Verhaak RG, McKenna A, Campos B, Noushmehr H, Salama SR*, et al.* The
823 somatic genomic landscape of glioblastoma. Cell **2013**;155(2):462-77 doi
824 10.1016/j.cell.2013.09.034.
825 4. Cruz Da Silva E, Mercier MC, Etienne-Selloum N, Dontenwill M, Choulier L. A
826 Systematic Review of Glioblastoma-Targeted Therapies in Phases II, III, IV Clinical
827 Trials. Cancers (Basel) **2021**;13(8) doi 10.3390/cancers13081795.
828 5. Dunn GP, Rinne ML, Wykosky J, Genovese G, Quayle SN, Dunn IF*, et al.* Emerging
829 insights into the molecular and cellular basis of glioblastoma. Genes Dev
830 **2012**;26(8):756-84 doi 10.1101/gad.187922.112.
831 6. Shen S, Vagner S, Robert C. Persistent Cancer Cells: The Deadly Survivors. Cell
832 **2020**;183(4):860-74 doi 10.1016/j.cell.2020.10.027.
833 7. Konieczkowski DJ, Johannessen CM, Garraway LA. A Convergence-Based Framework
834 for Cancer Drug Resistance. Cancer Cell **2018**;33(5):801-15 doi
835 10.1016/j.ccell.2018.03.025.

836 8. Smith MP, Wellbrock C. Molecular Pathways: Maintaining MAPK Inhibitor Sensitivity
837 by Targeting Nonmutational Tolerance. Clin Cancer Res **2016**;22(24):5966-70 doi
838 10.1158/1078-0432.CCR-16-0954.
839 9. Westermarck J. Targeted therapies don't work for a reason; the neglected tumor
840 suppressor phosphatase PP2A strikes back. FEBS J **2018**;285(22):4139-45 doi
841 10.1111/febs.14617.
842 10. Klaeger S, Heinzlmeir S, Wilhelm M, Polzer H, Vick B, Koenig PA*, et al.* The target
843 landscape of clinical kinase drugs. Science **2017**;358(6367) doi
844 10.1126/science.aan4368.
845 11. Lin A, Giuliano CJ, Palladino A, John KM, Abramowicz C, Yuan ML*, et al.* Off-target
846 toxicity is a common mechanism of action of cancer drugs undergoing clinical trials.
847 Science translational medicine **2019**;11(509) doi 10.1126/scitranslmed.aaw8412.
848 12. Montoya S, Soong D, Nguyen N, Affer M, Munamarty SP, Taylor J. Targeted Therapies
849 in Cancer: To Be or Not to Be, Selective. Biomedicines **2021**;9(11) doi
850 10.3390/biomedicines9111591.
851 13. Gani OA, Engh RA. Protein kinase inhibition of clinically important staurosporine
852 analogues. Natural product reports **2010**;27(4):489-98 doi 10.1039/b923848b.
853 14. Tang J, Tanoli ZUR, Ravikumar B, Alam Z, Rebane A, Vaha-Koskela M*, et al.* Drug Target
854 Commons: A Community Effort to Build a Consensus Knowledge Base for Drug-Target
855 Interactions. Cell Chem Biol **2018**;25(2):224-+ doi 10.1016/j.chembiol.2017.11.009.
856 15. Gimple RC, Bhargava S, Dixit D, Rich JN. Glioblastoma stem cells: lessons from the
857 tumor hierarchy in a lethal cancer. Genes Dev **2019**;33(11-12):591-609 doi
858 10.1101/gad.324301.119.

859 16. Patel AP, Tirosh I, Trombetta JJ, Shalek AK, Gillespie SM, Wakimoto H*, et al.* Single-cell
860 RNA-seq highlights intratumoral heterogeneity in primary glioblastoma. Science
861 **2014**;344(6190):1396-401 doi 10.1126/science.1254257.
862 17. Hoxhaj G, Manning BD. The PI3K-AKT network at the interface of oncogenic signalling
863 and cancer metabolism. Nature Reviews Cancer **2020**;20(2):74-88 doi
864 10.1038/s41568-019-0216-7.
865 18. Agnihotri S, Zadeh G. Metabolic reprogramming in glioblastoma: the influence of
866 cancer metabolism on epigenetics and unanswered questions. Neuro-oncology
867 **2016**;18(2):160-72 doi 10.1093/neuonc/nov125.
868 19. Michelakis ED, Sutendra G, Dromparis P, Webster L, Haromy A, Niven E*, et al.*
869 Metabolic modulation of glioblastoma with dichloroacetate. Science translational
870 medicine **2010**;2(31):31ra4 doi 10.1126/scitranslmed.3000677.
871 20. Wang Z, Peet NP, Zhang P, Jiang Y, Rong L. Current Development of Glioblastoma
872 Therapeutic Agents. Molecular cancer therapeutics **2021**;20(9):1521-32 doi
873 10.1158/1535-7163.MCT-21-0159.
874 21. Alexandru O, Horescu C, Sevastre AS, Cioc CE, Baloi C, Oprita A*, et al.* Receptor tyrosine
875 kinase targeting in glioblastoma: performance, limitations and future approaches.
876 Contemp Oncol (Pozn) **2020**;24(1):55-66 doi 10.5114/wo.2020.94726.
877 22. Kauko O, Westermarck J. Non-genomic mechanisms of protein phosphatase 2A (PP2A)
878 regulation in cancer. Int J Biochem Cell Biol **2018**;96:157-64 doi
879 10.1016/j.biocel.2018.01.005.
880 23. Fowle H, Zhao Z, Grana X. PP2A holoenzymes, substrate specificity driving cellular
881 functions and deregulation in cancer. Adv Cancer Res **2019**;144:55-93 doi
882 10.1016/bs.acr.2019.03.009.

883 24. Kauko O, O'Connor CM, Kulesskiy E, Sangodkar J, Aakula A, Izadmehr S*, et al.* PP2A
884 inhibition is a druggable MEK inhibitor resistance mechanism in KRAS-mutant lung
885 cancer cells. Science translational medicine **2018**;10(450) doi
886 10.1126/scitranslmed.aaq1093.
887 25. Merisaari J, Denisova OV, Doroszko M, Le Joncour V, Johansson P, Leenders WPJ*, et*
888 *al.* Monotherapy efficacy of blood-brain barrier permeable small molecule
889 reactivators of protein phosphatase 2A in glioblastoma. Brain Communications
890 **2020**;2(1) doi ARTN 02 10.1093/braincomms/fcaa002.
891 26. Qin S, Li J, Si Y, He Z, Zhang T, Wang D*, et al.* Cucurbitacin B induces inhibitory effects
892 via CIP2A/PP2A/Akt pathway in glioblastoma multiforme. Mol Carcinog
893 **2018**;57(6):687-99 doi 10.1002/mc.22789.
894 27. Puustinen P, Junttila MR, Vanhatupa S, Sablina AA, Hector ME, Teittinen K*, et al.* PME-
895 1 Protects Extracellular Signal-Regulated Kinase Pathway Activity from Protein
896 Phosphatase 2A-Mediated Inactivation in Human Malignant Glioma. Cancer Research
897 **2009**;69(7):2870-7 doi 10.1158/0008-5472.Can-08-2760.
898 28. Kaur A, Denisova OV, Qiao X, Jumppanen M, Peuhu E, Ahmed SU*, et al.* PP2A Inhibitor
899 PME-1 Drives Kinase Inhibitor Resistance in Glioma Cells. Cancer Research
900 **2016**;76(23):7001-11 doi 10.1158/0008-5472.Can-16-1134.
901 29. Vainonen JP, Momeny M, Westermarck J. Druggable cancer phosphatases. Science
902 translational medicine **2021**;13(588) doi 10.1126/scitranslmed.abe2967.
903 30. Akimov Y, Aittokallio T. Re-defining synthetic lethality by phenotypic profiling for
904 precision oncology. Cell Chem Biol **2021**;28(3):246-56 doi
905 10.1016/j.chembiol.2021.01.026.

906 31. Kaur A, Westermarck J. Regulation of protein phosphatase 2A (PP2A) tumor
907 suppressor function by PME-1. Biochem Soc Trans **2016**;44(6):1683-93 doi
908 10.1042/BST20160161.
909 32. Sangodkar J, Perl A, Tohme R, Kiselar J, Kastrinsky DB, Zaware N*, et al.* Activation of
910 tumor suppressor protein PP2A inhibits KRAS-driven tumor growth. J Clin Invest
911 **2017**;127(6):2081-90 doi 10.1172/JCI89548.
912 33. Vit G, Duro J, Rajendraprasad G, Hertz EPT, Kauffeldt Holland LK, Weisser MB*, et al.*
913 Cellular toxicity of iHAP1 and DT-061 does not occur through PP2A-B56 targeting.
914 bioRxiv **2021**:2021.07.08.451586 doi 10.1101/2021.07.08.451586.
915 34. Taipale M. Quantitative Profiling of Chaperone/Client Interactions with LUMIER Assay.
916 Methods Mol Biol **2018**;1709:47-58 doi 10.1007/978-1-4939-7477-1_4.
917 35. Taipale M, Krykbaeva I, Whitesell L, Santagata S, Zhang J, Liu Q*, et al.* Chaperones as
918 thermodynamic sensors of drug-target interactions reveal kinase inhibitor specificities
919 in living cells. Nature biotechnology **2013**;31(7):630-7 doi 10.1038/nbt.2620.
920 36. Shariati M, Meric-Bernstam F. Targeting AKT for cancer therapy. Expert Opin Investig
921 Drugs **2019**;28(11):977-88 doi 10.1080/13543784.2019.1676726.
922 37. Stacpoole PW. Therapeutic Targeting of the Pyruvate Dehydrogenase
923 Complex/Pyruvate Dehydrogenase Kinase (PDC/PDK) Axis in Cancer. Journal of the
924 National Cancer Institute **2017**;109(11) doi 10.1093/jnci/djx071.
925 38. Le Joncour V, Filppu P, Hyvonen M, Holopainen M, Turunen SP, Sihto H*, et al.*
926 Vulnerability of invasive glioblastoma cells to lysosomal membrane destabilization.
927 EMBO Mol Med **2019**;11(6) doi 10.15252/emmm.201809034.

928 39. Mooney J, Bernstock JD, Ilyas A, Ibrahim A, Yamashita D, Markert JM*, et al.* Current
929 Approaches and Challenges in the Molecular Therapeutic Targeting of Glioblastoma.
930 World Neurosurg **2019**;129:90-100 doi 10.1016/j.wneu.2019.05.205.
931 40. Wen J, Hadden MK. Medulloblastoma drugs in development: Current leads, trials and
932 drawbacks. Eur J Med Chem **2021**;215:113268 doi 10.1016/j.ejmech.2021.113268.
933 41. Di Magno L, Manzi D, D'Amico D, Coni S, Macone A, Infante P*, et al.* Druggable
934 glycolytic requirement for Hedgehog-dependent neuronal and medulloblastoma
935 growth. Cell Cycle **2014**;13(21):3404-13 doi 10.4161/15384101.2014.952973.
936 42. Austin JA, Jenkins RE, Austin GM, Glenn MA, Dunn K, Scott L*, et al.* Cancerous inhibitor
937 of protein phosphatase 2A (CIP2A) modifies energy metabolism via 5' AMP-activated
938 protein kinase signalling in malignant cells. Biochem J **2019**;476(15):2255-69 doi
939 10.1042/BCJ20190121.
940 43. Atas E, Oberhuber M, Kenner L. The Implications of PDK1-4 on Tumor Energy
941 Metabolism, Aggressiveness and Therapy Resistance. Frontiers in oncology
942 **2020**;10:583217 doi 10.3389/fonc.2020.583217.
943 44. Bosc C, Saland E, Bousard A, Gadaud G, Sabatier M, Cognet G*, et al.* Mitochondrial
944 inhibitors circumvent adaptive resistance to venetoclax and cytarabine combination
945 therapy in acute myeloid leukemia. Nature Cancer **2021**;2:1204–23.
946 45. Potter DS, Letai A. To Prime, or Not to Prime: That Is the Question. Cold Spring Harbor
947 symposia on quantitative biology **2016**;81:131-40 doi 10.1101/sqb.2016.81.030841.
948 46. Koch R, Christie AL, Crombie JL, Palmer AC, Plana D, Shigemori K*, et al.* Biomarker-
949 driven strategy for MCL1 inhibition in T-cell lymphomas. Blood **2019**;133(6):566-75 doi
950 10.1182/blood-2018-07-865527.

951 47. Ryan J, Montero J, Rocco J, Letai A. iBH3: simple, fixable BH3 profiling to determine
952 apoptotic priming in primary tissue by flow cytometry. Biol Chem **2016**;397(7):671-8
953 doi 10.1515/hsz-2016-0107.
954 48. Xie Q, Wu Q, Kim L, Miller TE, Liau BB, Mack SC*, et al.* RBPJ maintains brain tumor-
955 initiating cells through CDK9-mediated transcriptional elongation. J Clin Invest
956 **2016**;126(7):2757-72 doi 10.1172/JCI86114.
957 49. Vervoort SJ, Welsh SA, Devlin JR, Barbieri E, Knight DA, Offley S*, et al.* The PP2A-
958 Integrator-CDK9 axis fine-tunes transcription and can be targeted therapeutically in
959 cancer. Cell **2021**;184(12):3143-62 e32 doi 10.1016/j.cell.2021.04.022.
960 50. Dhanasekaran DN, Reddy EP. JNK signaling in apoptosis. Oncogene **2008**;27(48):6245-
961 51 doi 10.1038/onc.2008.301.
962 51. Kaley TJ, Panageas KS, Mellinghoff IK, Nolan C, Gavrilovic IT, DeAngelis LM*, et al.* Phase
963 II trial of an AKT inhibitor (perifosine) for recurrent glioblastoma. J Neurooncol
964 **2019**;144(2):403-7 doi 10.1007/s11060-019-03243-7.
965 52. Wen PY, Touat M, Alexander BM, Mellinghoff IK, Ramkissoon S, McCluskey CS*, et al.*
966 Buparlisib in Patients With Recurrent Glioblastoma Harboring Phosphatidylinositol 3-
967 Kinase Pathway Activation: An Open-Label, Multicenter, Multi-Arm, Phase II Trial. J
968 Clin Oncol **2019**;37(9):741-50 doi 10.1200/JCO.18.01207.
969 53. Dunbar EM, Coats BS, Shroads AL, Langaee T, Lew A, Forder JR*, et al.* Phase 1 trial of
970 dichloroacetate (DCA) in adults with recurrent malignant brain tumors. Investigational
971 new drugs **2014**;32(3):452-64 doi 10.1007/s10637-013-0047-4.
972 54. Oshima N, Ishida R, Kishimoto S, Beebe K, Brender JR, Yamamoto K*, et al.* Dynamic
973 Imaging of LDH Inhibition in Tumors Reveals Rapid In Vivo Metabolic Rewiring and

974 Vulnerability to Combination Therapy. Cell reports **2020**;30(6):1798-810 e4 doi
975 10.1016/j.celrep.2020.01.039.
976 55. Ly JD, Grubb DR, Lawen A. The mitochondrial membrane potential (deltapsi(m)) in
977 apoptosis; an update. Apoptosis **2003**;8(2):115-28 doi 10.1023/a:1022945107762.
978 56. Garner EF, Williams AP, Stafman LL, Aye JM, Mroczek-Musulman E, Moore BP*, et al.*
979 FTY720 Decreases Tumorigenesis in Group 3 Medulloblastoma Patient-Derived
980 Xenografts. Scientific reports **2018**;8(1):6913 doi 10.1038/s41598-018-25263-5.
981 57. Guzman C, Bagga M, Kaur A, Westermarck J, Abankwa D. ColonyArea: an ImageJ plugin
982 to automatically quantify colony formation in clonogenic assays. PloS one
983 **2014**;9(3):e92444 doi 10.1371/journal.pone.0092444.
984 58. Shannon P, Markiel A, Ozier O, Baliga NS, Wang JT, Ramage D*, et al.* Cytoscape: a
985 software environment for integrated models of biomolecular interaction networks.
986 Genome research **2003**;13(11):2498-504.
987 59. Szklarczyk D, Gable AL, Nastou KC, Lyon D, Kirsch R, Pyysalo S*, et al.* The STRING
988 database in 2021: customizable protein-protein networks, and functional
989 characterization of user-uploaded gene/measurement sets. Nucleic Acids Res
990 **2021**;49(D1):D605-D12 doi 10.1093/nar/gkaa1074.
991 60. Ianevski A, Giri AK, Aittokallio T. SynergyFinder 2.0: visual analytics of multi-drug
992 combination synergies. Nucleic Acids Res **2020**;48(W1):W488-W93 doi
993 10.1093/nar/gkaa216.
994